Effect of Processing Conditions on the Structure Development in the Welding Region of Injection-Molded Poly(Arylene Ether Ketone). III

Y. ULCER, M. CAKMAK,* and C. M. HSIUNG

Institute of Polymer Engineering, College of Polymer Engineering and Polymer Science, University of Akron, Akron, Ohio 44325-0301

SYNOPSIS

Effect of injection-molding process conditions including mold temperature and injection speed on the structure developed at the weld region of poly(arylene ether ketone) was investigated using MMBX (matrixing micro beam X-ray diffraction) and image analysis techniques. The polymer exhibited multilayer structural formations at and near the weld region, and these were found to be alternating highly crystalline and low crystalline regions. With the exception of the converging section of the cavity, no significant orientations were observed through the X-ray diffraction method. However, polarized light microscopy studies revealed that the bands of higher crystallinity possess higher birefringence as compared to the intervening regions. This suggested that these bands are formed under an orientational flow field. The geometrical pattern of these multilayer formations changes depending on the injection-molding condition particularly with injection speed and mold temperature. Tensile test results indicate that the samples with no weld regions generally possess higher tensile strength. This difference between the tensile properties of the samples possessing weld and no weld decreases at high injection speeds. Izod impact strength exhibited an unusual behavior: The welded parts actually possess higher impact strength. This was attributed to the formation of multilayer structures at the weld zone. © 1995 John Wiley & Sons, Inc.

INTRODUCTION

The weld line in most injection-molded polymers plays an important role in determining the performance characteristics of the part. They can be formed due to several factors causing stagnation points or uneven (unbalanced) mold filling in multiple gated complex mold geometries. However, the most frequently encountered cases of weld line formation are (i) recombination of a polymer melt stream after flowing around the obstacles present in the flow direction and (ii) meeting of various melt streams originating from different gates. In either case weld line formation causes severe reduction in mechanical and surface properties.[1,2]

Poly(arylene ether ketone) (PAEK) is a polymer with slow crystallization characteristics due to its semirigid backbone structure that includes aromatic groups. This characteristic results in molded parts having complex structural gradients across and along the flow directions[3] similar to poly-*p*-phenylene sulfide and poly(ether ether ketone).[4,5] In our earlier studies[3-5] we showed that when PAEK is molded into thin cavities where high cooling rates are attained, three layered—amorphous skin, semicrystalline intermediate later, and amorphous core structural gradients are formed through the thickness of the parts. If the cavity thickness or mold temperature is increased, the crystallinity increases monotonously from skin to core regions of the samples. At very high mold temperatures where substantial thermally activated crystallization rates are attained, the crystallinity becomes uniformly high and minimal crystallinity gradient is observed.

* To whom correspondence should be addressed.

Journal of Applied Polymer Science, Vol. 55, 1241–1263 (1995)
 CCC 0021-8995/95/081241-23

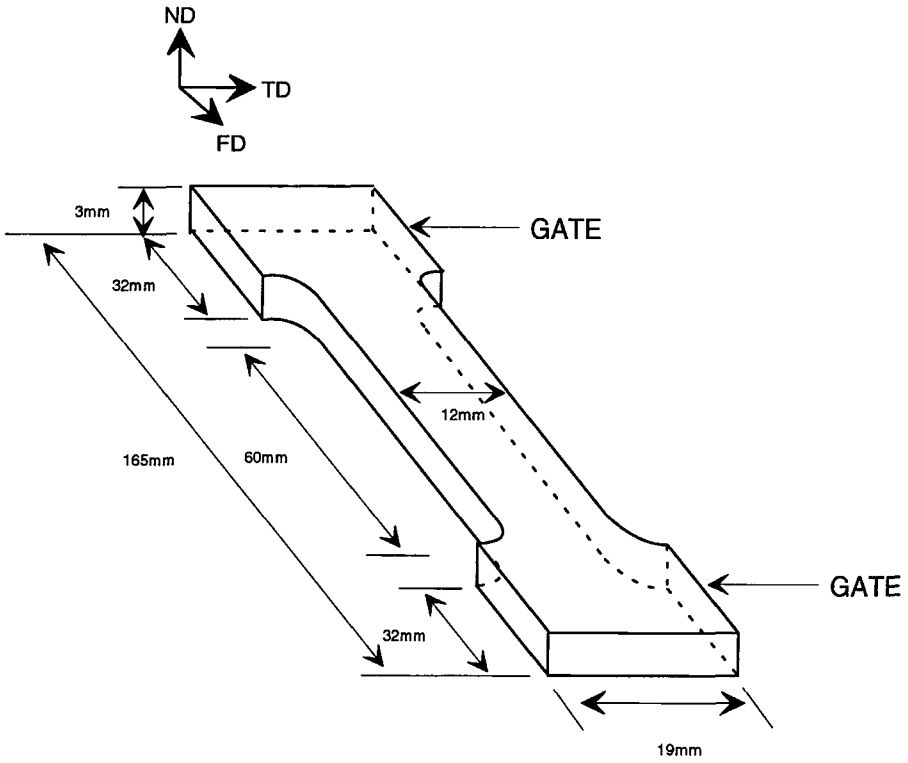

Figure 1 Schematic diagram of mold cavity.

In this work, we present our studies on the influence of processing variables on the structural development in the weld region of PAEK parts produced using a double-gated cavity.

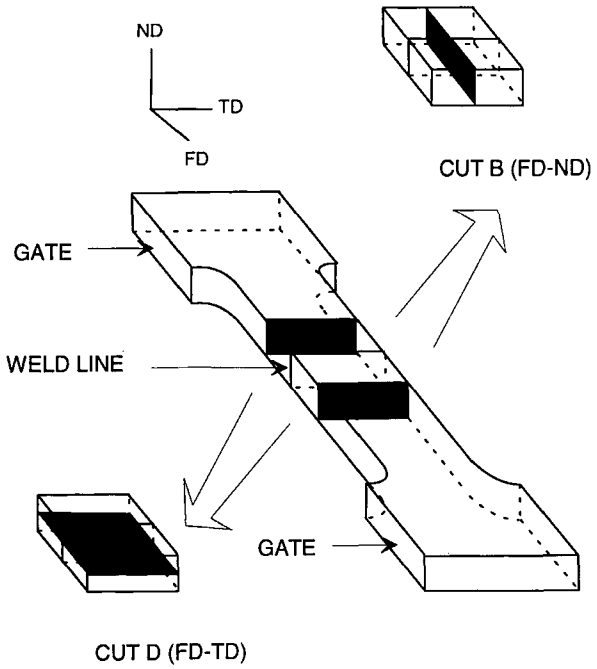

Figure 2 Schematics of cutting procedures.

EXPERIMENTAL

Materials

Poly(arylene ether ketone) KADEL E1000 was obtained from Amoco Corporation. The pelletized samples were dried in a vacuum oven for 12 h at 130°C before their use. Relevant rheological and thermal properties of this polymer were reported in our earlier study.[6]

Injection Molding

In this study large ASTM tensile bars of 3 mm thickness (Fig. 1) were injection molded using a BOY (Model 15S) 15-ton reciprocating-screw injection-molding machine equipped with a mold with a double-ended cavity. The temperature of the mold was controlled by an oil circulating mold temperature controller. The injection speed was monitored by a linear variable differential transformer (LVDT) connected to the screw section on the forward drive.

To investigate the effect of barrel temperature (T_b) on the weld line structure, parts were molded at 370 and 400°C melt temperatures. Using these two melt temperatures, the parts were made at mold temperatures of 20, 150, and 200°C (T_m). Two in-

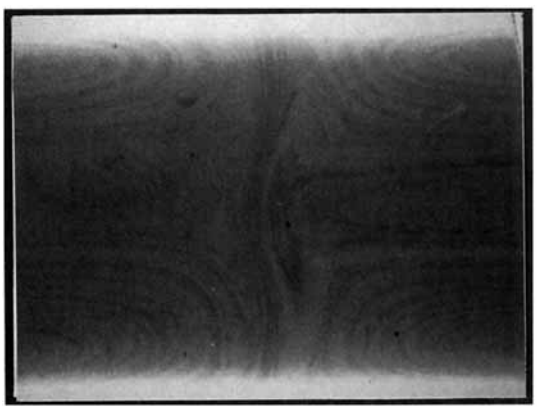

T_b=370°C T_m=150°C
Injection Speed=5.2 cm³/s

T_b=370°C T_m=150°C
Injection Speed=23.2 cm³/s

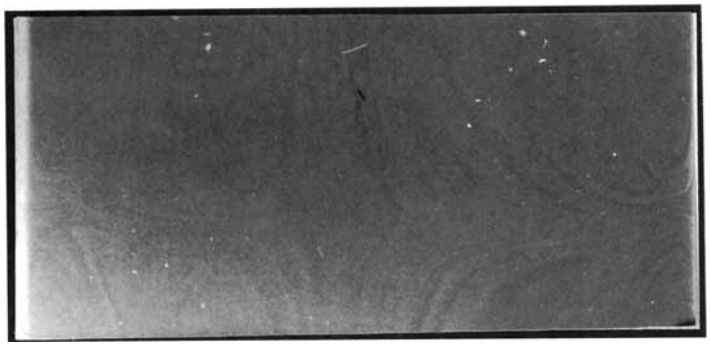

T_b=370°C T_m=150°C
Injection Speed=5.2 cm³/s

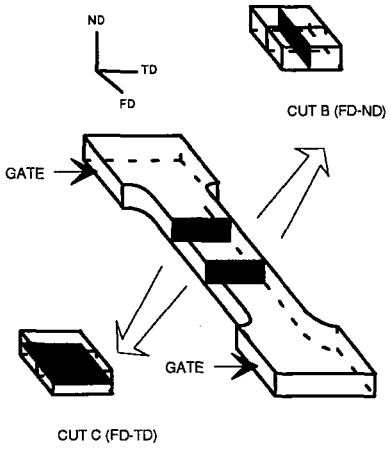

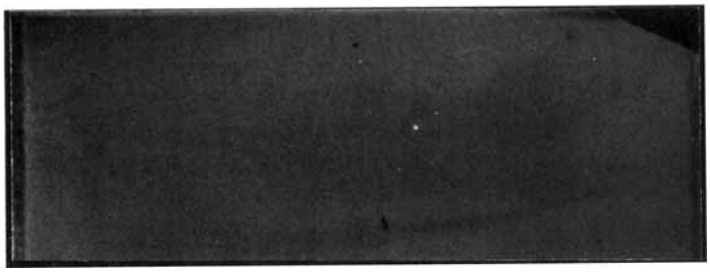

T_b=370°C T_m=150°C
Injection Speed=23.2 cm³/s

Figure 3 Weld structure of samples cut with procedure B and C unprocessed images. (a) T_b = 370°C and T_m = 150°C, B cut, (b) T_b = 400°C and T_m = 150°C, C cut.

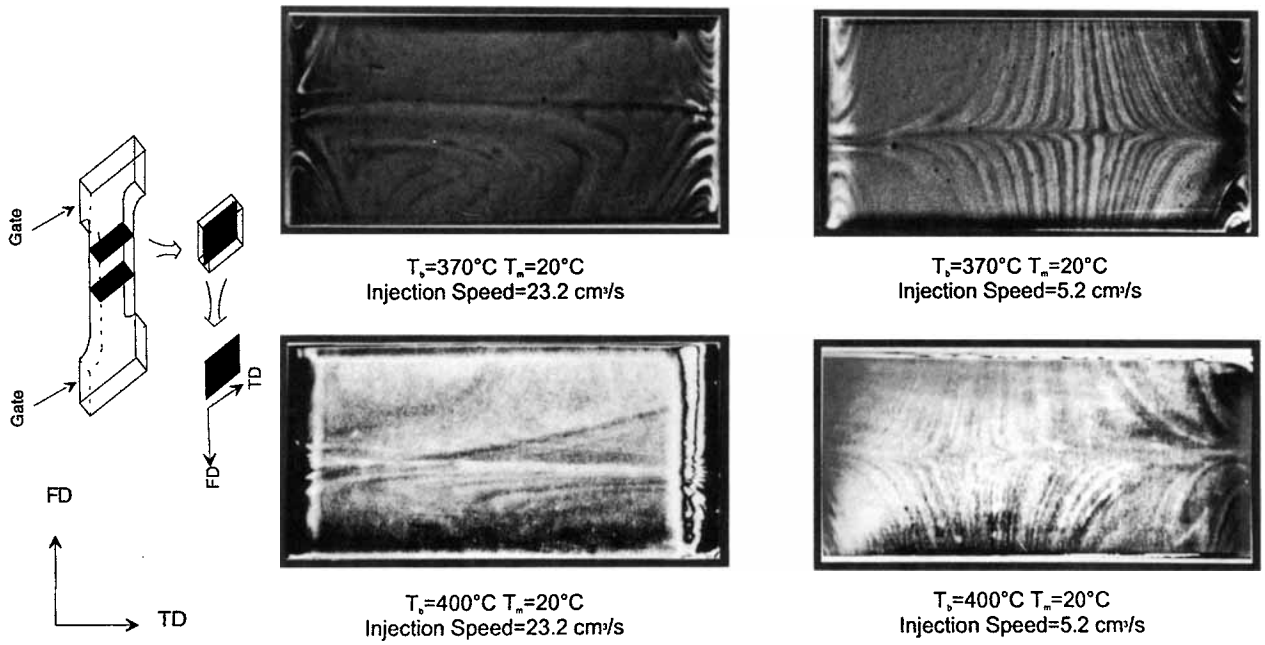

Figure 4 Weld structure of samples cut with procedure C. (a) T_b = 370°C and T_m = 20°C, (b) T_b = 400°C and T_m = 20°C.

jection speeds were utilized to mold the samples. These are designated as "low speed," where the average melt flow rate was 5.2 cm^3/s, and a "high speed," where the average melt flow rate was 23.2 cm^3/s. Both injection and back pressure were kept constant at 13.7 and 1.37 MPa, respectively. The holding time was kept constant at 1 min for all the parts produced.

Sample Sectioning

To investigate the structural characteristics, the molded samples were sectioned using a Leco VC-50 variable-speed diamond saw and a Reichert-Jung 2050 microtome. Two different cutting procedures were used (Fig. 2): (i) procedure B consists of slicing the sample along the flow direction at the flow direction–normal direction (FD–ND) symmetry plane and (ii) procedure C consists of slicing the sample across the flow direction at the flow direction–transverse direction (FD–TD) symmetry midplane. The planes of these two cuts are orthogonal to each other, enabling us to study the weld line structure from two perspectives.

Image Processing

Transmission optical photomicrographs of the slices cut by procedures B and C were captured using a Sony 3CCD video camera connected to a Sun 4/150 workstation. In order to investigate the fine details of the structures, the images were digitized and contrast enhanced using an image processing software.

In order to study the size and orientation changes in the weld zone, the melting sequence of the selected samples was recorded and analyzed. For this, the samples microtomed with procedure B at the weld region were placed in a Mettler FP84 hot stage cell and heated at 10°C/min while recording the polarized optical transmission image through the microscope using the video camera and a video recorder. During melting, selected images were captured and their transmitted depolarized light intensity histogram as well as their mean over the whole image field were obtained through image analysis.

Wide-Angle X-ray Diffraction Film Patterns by Matrixing Micro Beam X-ray Camera (MMBWAXD)

Details of the layer formation were investigated using a matrixing micro beam X-ray camera developed in our laboratories. The camera was mounted on a 12-kW Rigaku (RU 200B) rotating anode generator that was operated at 40 kV and 150 mA. The X-ray beam of 100 mm diameter was monochromatized using a nickel foil filter. The sample is mounted on

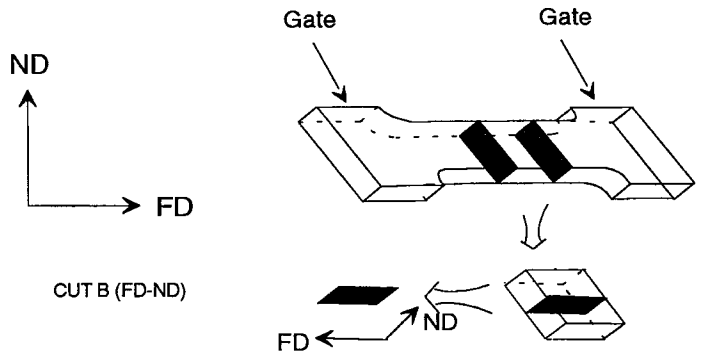

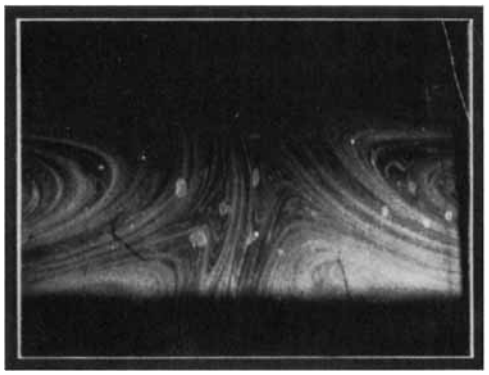

T_b=370°C T_m=20°C
Injection Speed=23.2 cm³/s

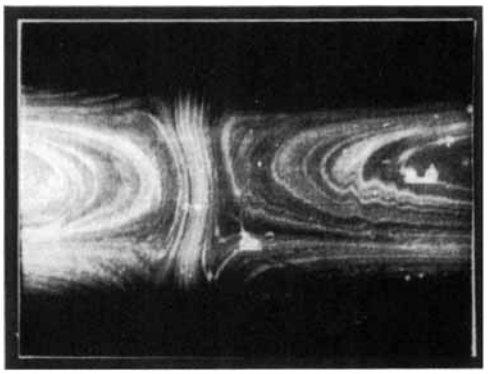

T_b=370°C T_m=20°C
Injection Speed=5.2 cm³/s

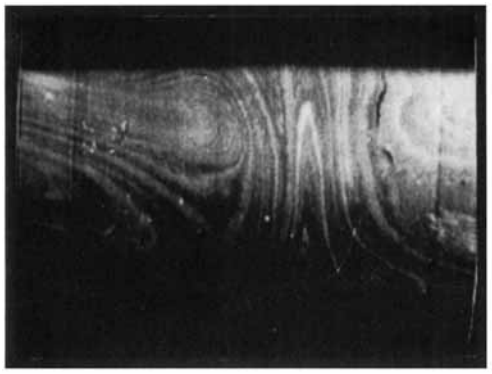

T_b=400°C T_m=20°C
Injection Speed=23.2 cm³/s

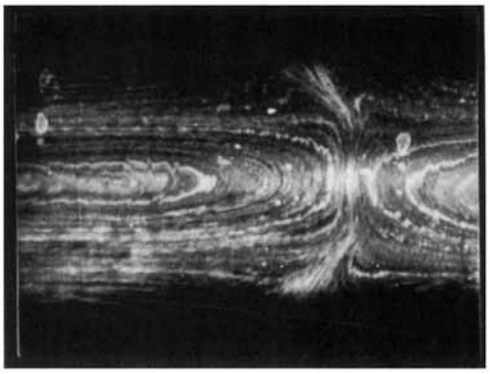

T_b=400°C T_m=20°C
Injection Speed=5.2 cm³/s

Figure 5 Weld structure of samples cut with procedure B. (a) T_b = 370°C and T_m = 20°C, (b) T_b = 400°C and T_m = 20°C.

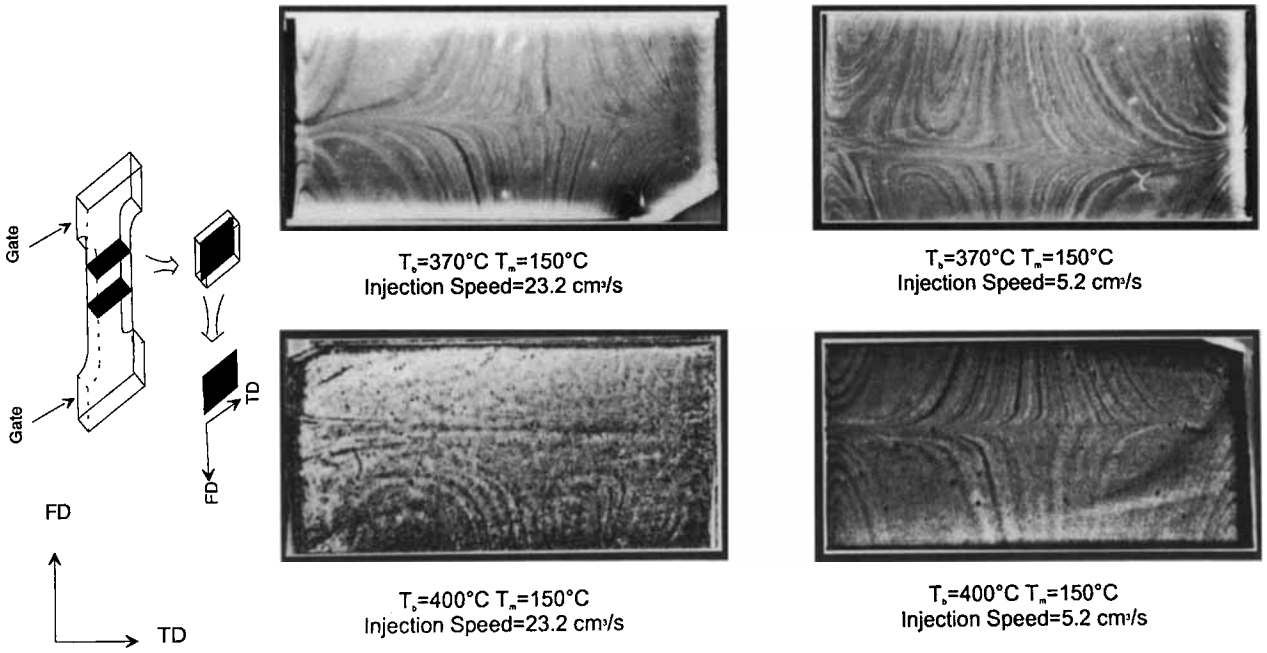

Figure 6 Weld structure of samples cut with procedure C. (a) T_b = 370°C and T_m = 150°C, (b) T_b = 400°C and T_m = 150°C.

a precision X-Y stage and WAXD film patterns were obtained at a series locations in the sample without dismounting. Typical exposure times were about 30 min.

Mechanical Properties

Tensile testing was performed using a Monsanto T-10 tensile tester with a testing rate of 5 mm/min and with an initial 100-mm gauge length. For each condition, the results obtained from seven specimens were averaged.

Impact Testing

Impact testing of the samples notched at the weld line was performed using a TMI impact tester at room temperature. The optical photomicrographs of fracture surfaces were taken by a Nikon SMZ-10 stereo microscope in reflection mode.

RESULTS AND DISCUSSION

Optical Photomicrographs

The optical photomicrographs of samples cut with procedures B and C are given in Figures 3 through 8 for a variety of processing conditions. Figure 3 shows typical unprocessed transmission photomicrographs taken from samples molded at T_m = 150°C and T_b = 370°C. We can see that although some substructural details are visible, the images lack overall contrast especially in the case of cuts made by procedure C. To achieve the necessary contrast and image quality, we performed a series of point (local histogram equalization + gamma correction + inversion and staircase threshold) and arithmetic (multiplication) operations on the digitized images. In all cases the first correction was a 16-pixel local equalization that compensated for the uneven illumination field due to the slight thickness variations. Then the images were inverted and gamma corrected to compensate for the nonlinear response characteristics of the video camera. Finally the resulting images were stretched to increase their contrast. However, for most of the samples cut with procedure C, an additional staircase thresholding step was required to obtain maximum contrast.

Figures 4 and 5 show the negatives of FD–TD and FD–ND planes of the weld region of samples molded at T_m = 20°C using different barrel temperatures and injection speeds. In the pictures showing FD–TD planes [4(a) and 4(b)] two melt fronts approach each other from the top and bottom of the picture and meet at the midsection, whereas in FD–ND case [5(a) and 5(b)] the flow fronts advance from

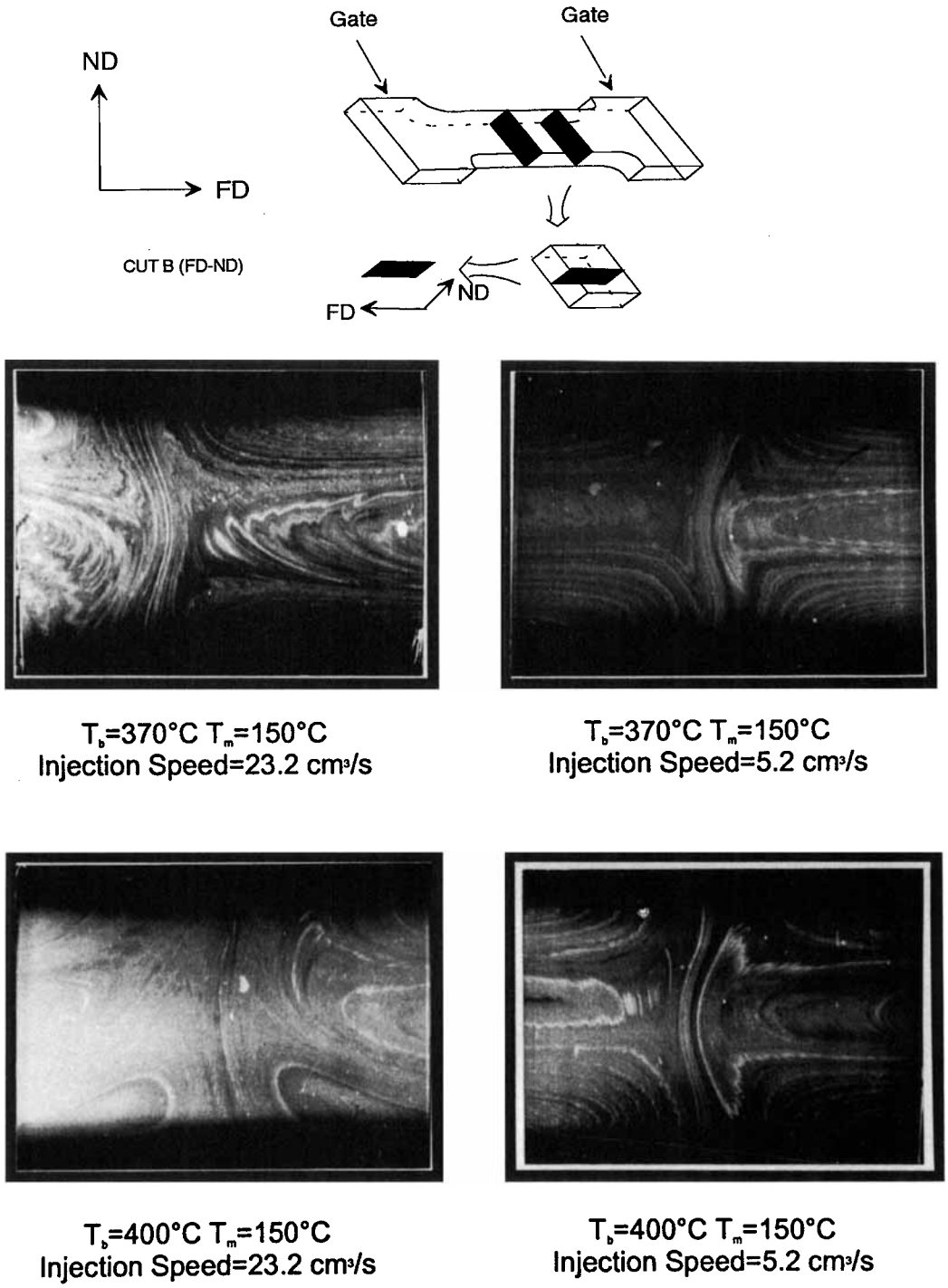

Figure 7 Weld structure of samples cut with procedure B. (a) T_b = 370°C and T_m = 150°C, (b) T_b = 400°C and T_m = 150°C.

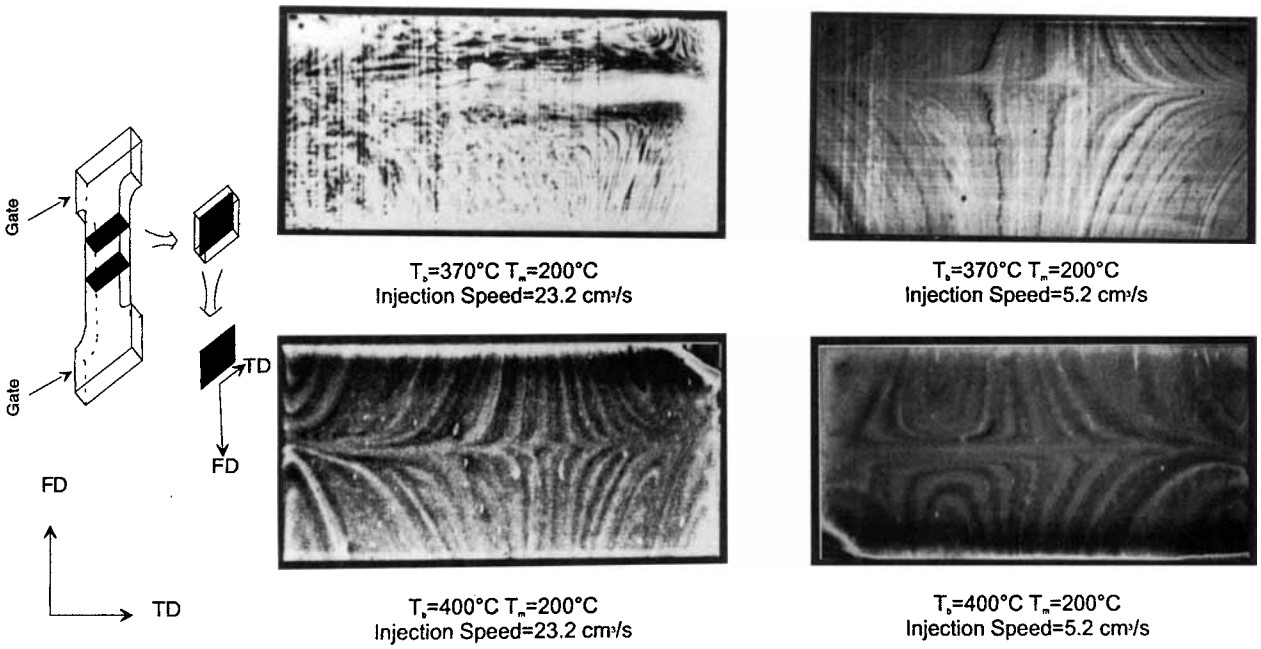

Figure 8 Weld structure of samples cut with procedure C. (a) T_b = 370°C and T_m = 200°C, (b) T_b = 400°C and T_m = 200°C.

right and left sides of the picture. We can distinguish numerous structural features: the skin region at this low mold temperature is transparent (the dark regions at the left and right side of C cuts and top and bottom parts of B cuts), and the appearance of the sample becomes opaque at the interior with dark-light alternating layers. In the FD–TD plane these multilayer formations extend further into the interior of the part when the samples are molded using the low injection speed, whereas in samples molded using the high speed, the layers parallel to the weld line are observed particularly in the sample molded with high melt temperature (T_b = 400°C). The shapes of the alternating layers in the FD–ND plane follow the parabolic profile of the flow field and the fountain flow effect. At low injection speeds the two melt fronts meet at moderate pressures and low momentum, which preserves the regular shape of the fountain flow patterns. However, there is significant buckling at high injection speeds. Further evidence supporting that these layers originate from the fountain flow comes from the observation that at lower injection speeds, the frozen layers become thicker during the flow. As a result, these layer formations extend further into the core of these specimens. In high-speed molded samples, on the other hand, the fountain effect is much less, particularly when the melt temperature is high. Consequently, the layer formations are not as pronounced. When the mold temperature was increased to temperatures at and above 150°C (Figs 6 to 8), we observed significant structural changes especially at samples molded with low injection speed. At this mold tem-

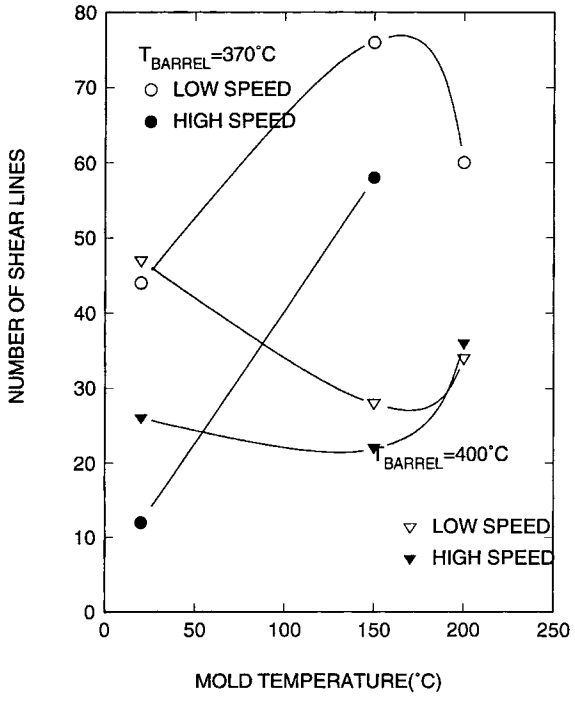

Figure 9 Number of shear lines counted along a line sufficiently away from the weld line.

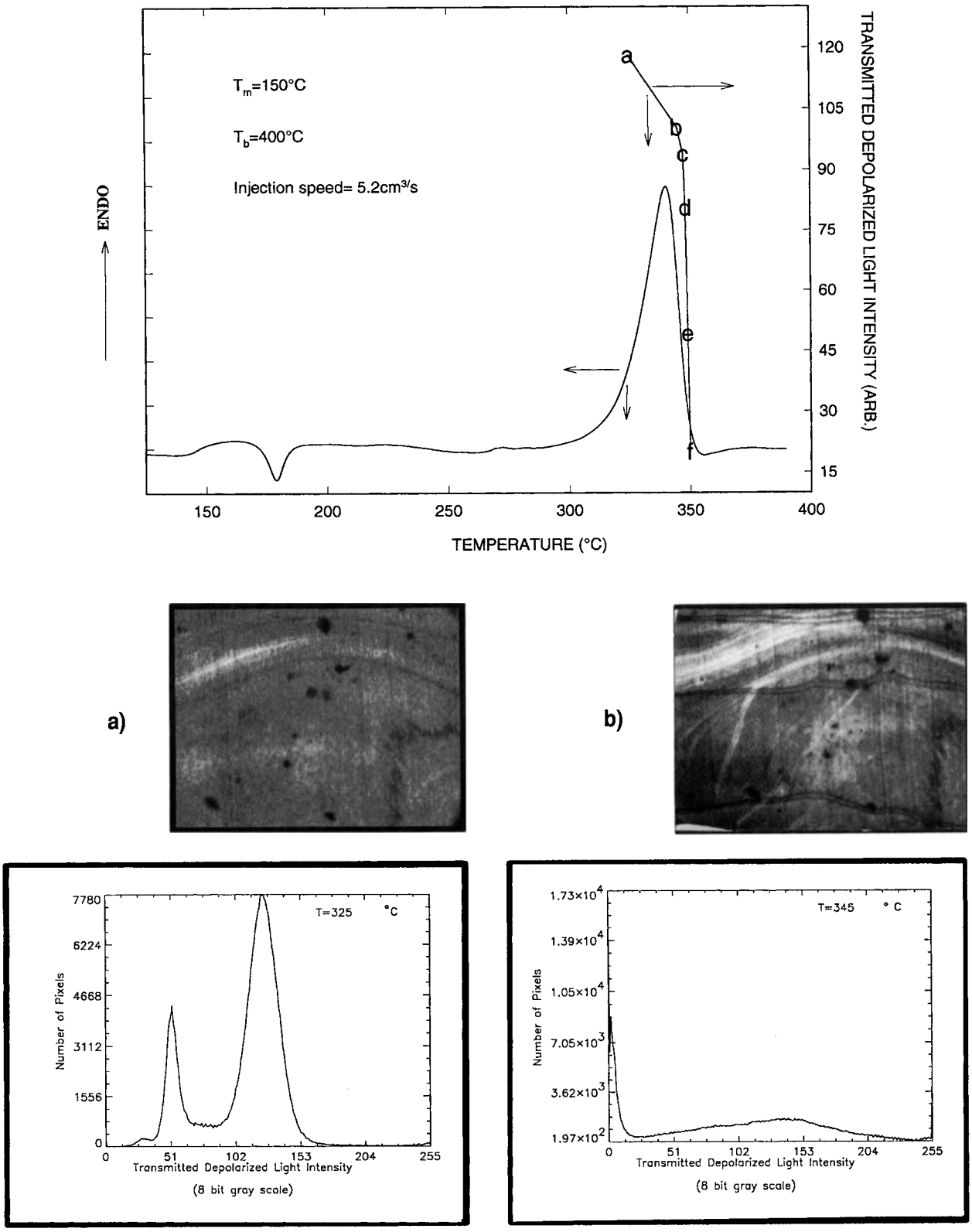

Figure 10 Analysis of the melting of a section cut with procedure B: (a) differential scanning calorimetry trace at the weldline and average intensity vs. temperature, (b) polarized photomicrographs taken at a series of temperatures during melting and corresponding transmitted depolarized light intensity histograms. T_b = 400°C, T_m = 150°C, and injection speed = 5.2 cm³/s.

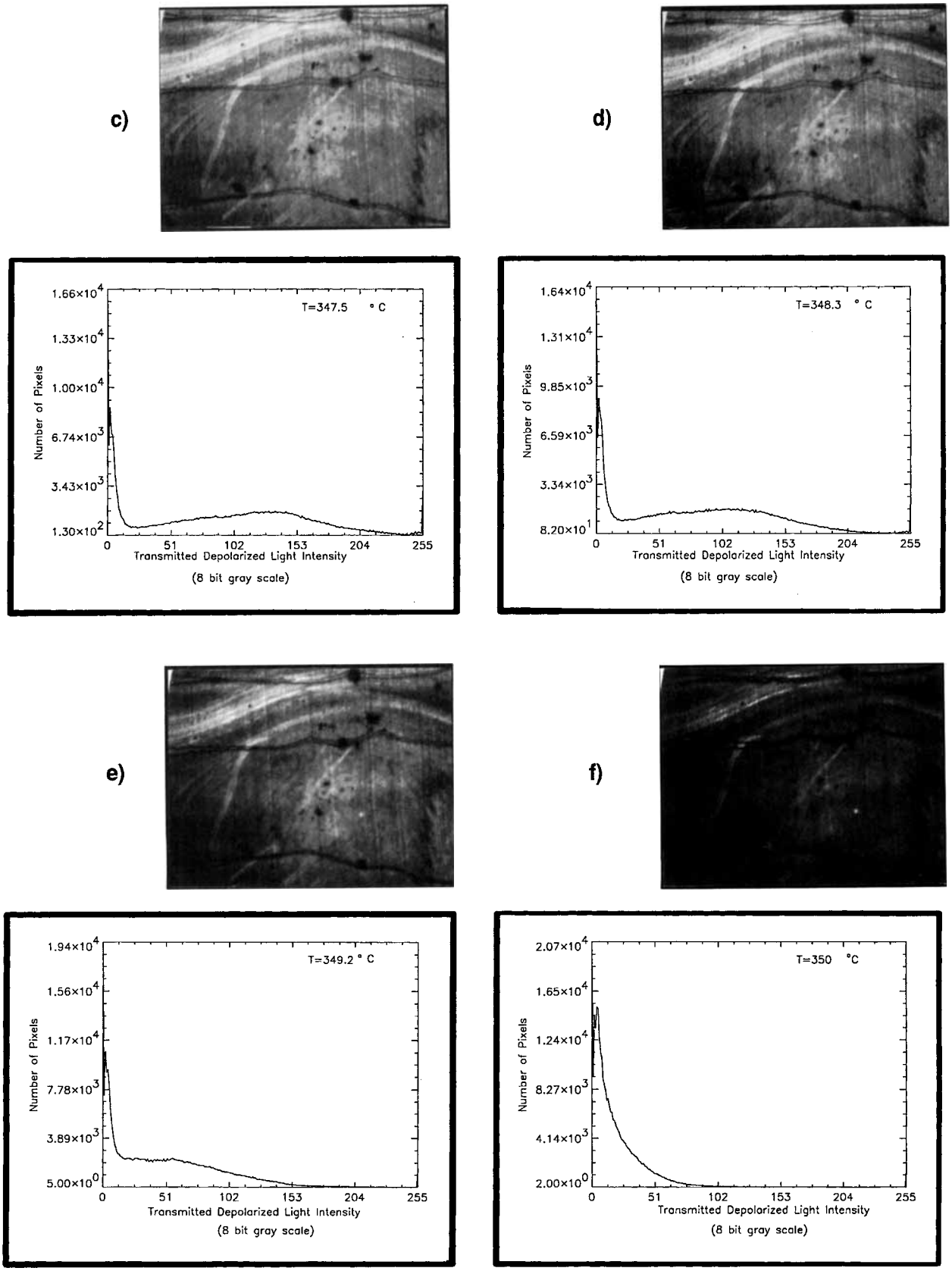

Figure 10 (*Continued from the previous page*)

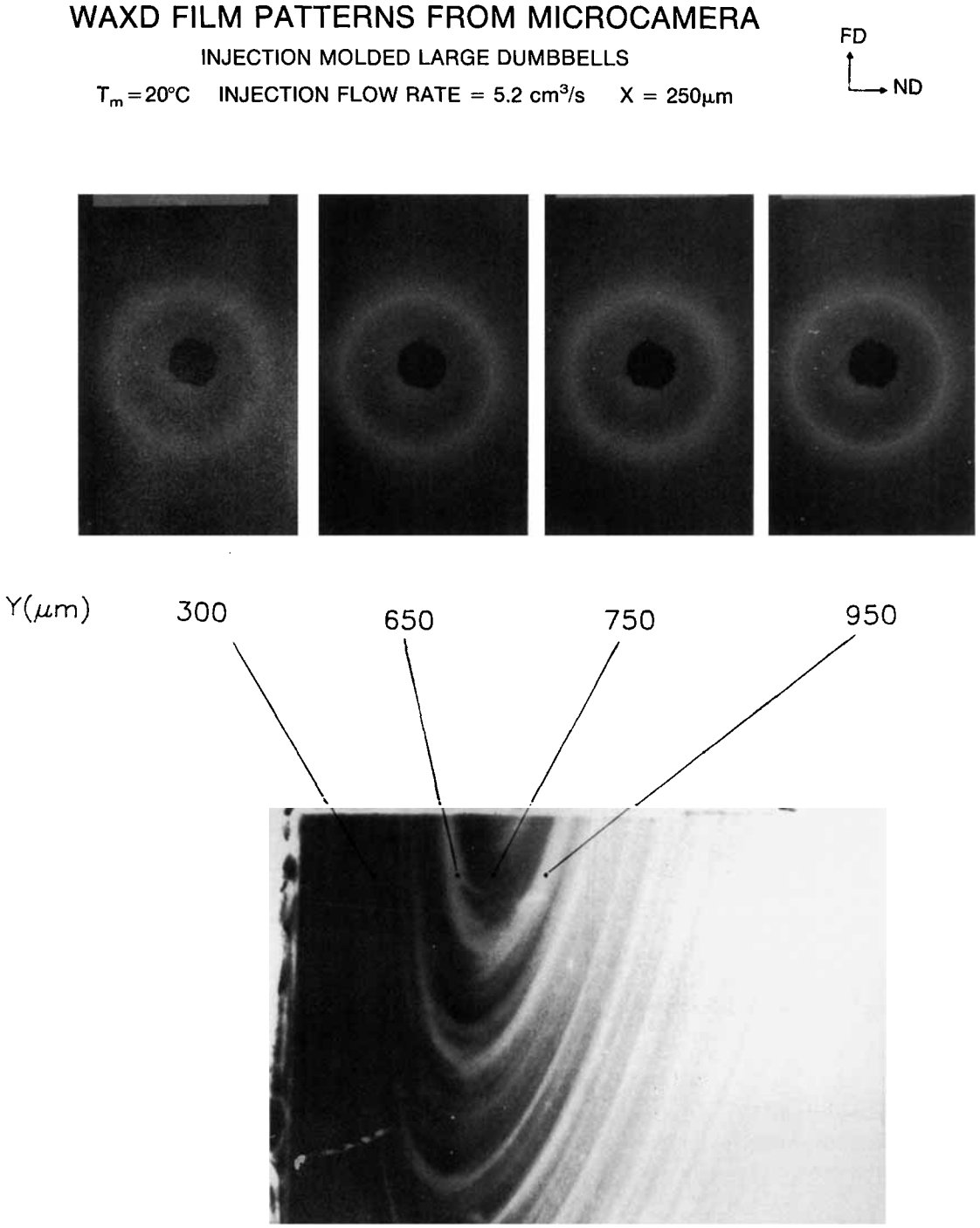

Figure 11 *Micro beam wide-angle X-ray diffraction patterns taken along the layered structure upstream from the weld line near the skin. Sample cut with procedure C,* T_b = 400°C, T_m = 20°C, and injection speed = 5.2 cm³/s.

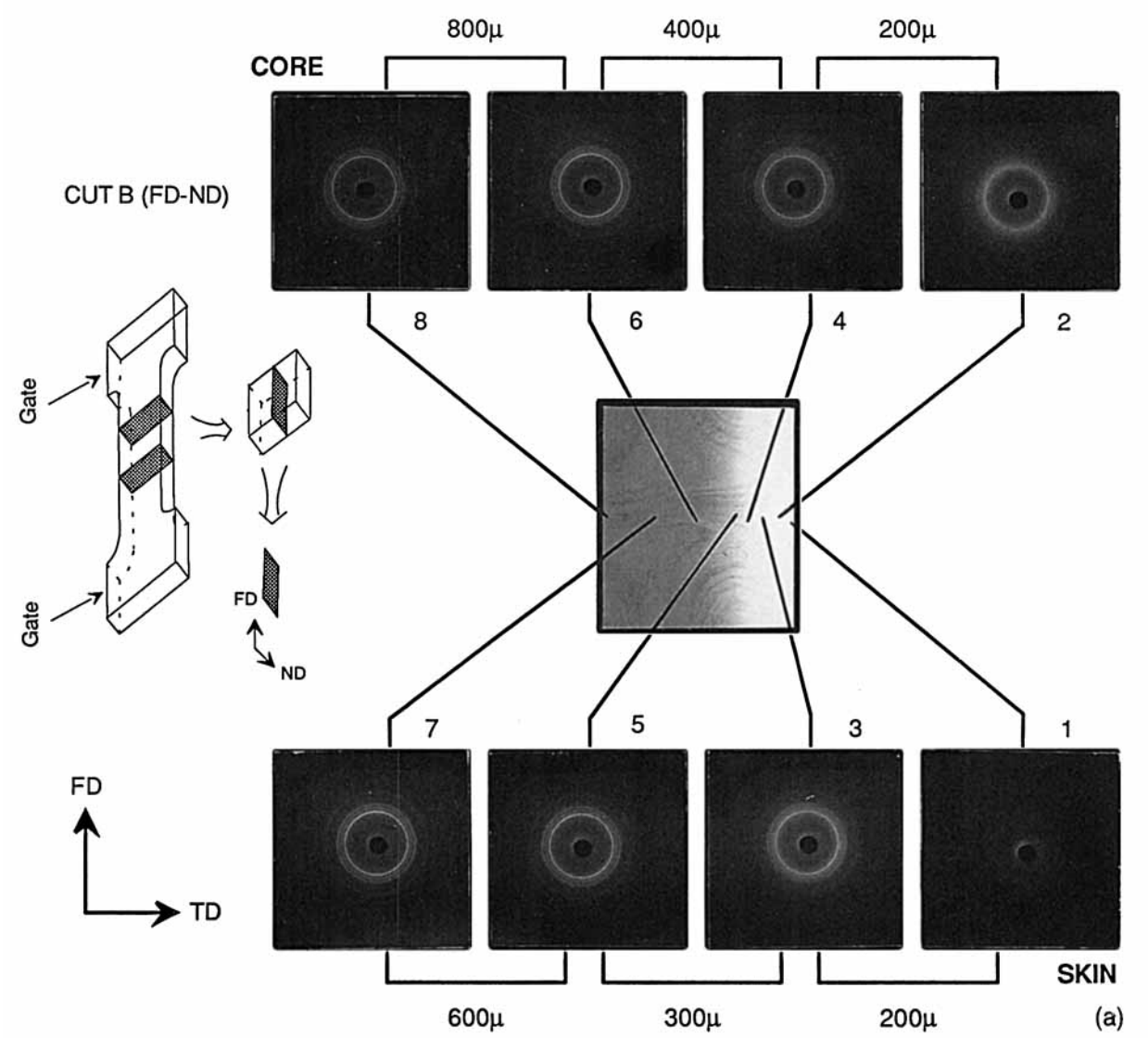

Figure 12 Micro beam wide-angle X-ray diffraction patterns through the weld line taken from a sample cut with procedure B. T_b = 370°C, T_m = 20°C. (a) Injection speed = 5.2 cm^3/s and (b) injection speed = 23.2 cm^3/s.

perature the material cools slower and consequently the progress of frozen layer development during the filling is greatly suppressed. This, in turn, lowers overall shear history. Due to the reduction of cooling rates, the amorphous transparent skin layer thickness also becomes smaller. We also noted that the number of alternating lines increase at low barrel temperature and with low injection speeds as shown in Figure 9.

To elucidate the origin of the alternating dark and light layers, we analyzed the melting sequence of a slice cut with procedure B form a sample molded at T_b = 400°C and T_m = 150°C with the low injection speed. Figure 10 summarizes the results of the analysis. Melting of the sample begins around 340°C, which is manifested by a reduction in the transmitted polarized light intensity. However, up to 350°C, which is at the high-temperature tail of the melting peak [see Fig. 10(a)], the layers remain birefringent. Above 354°C the birefringent layers begin to melt. This melting of the sublayers starts away from the weld zone and those that are locate at the weld zone melt the last. This local increase of melting temperature in the sublayer regions suggest that these

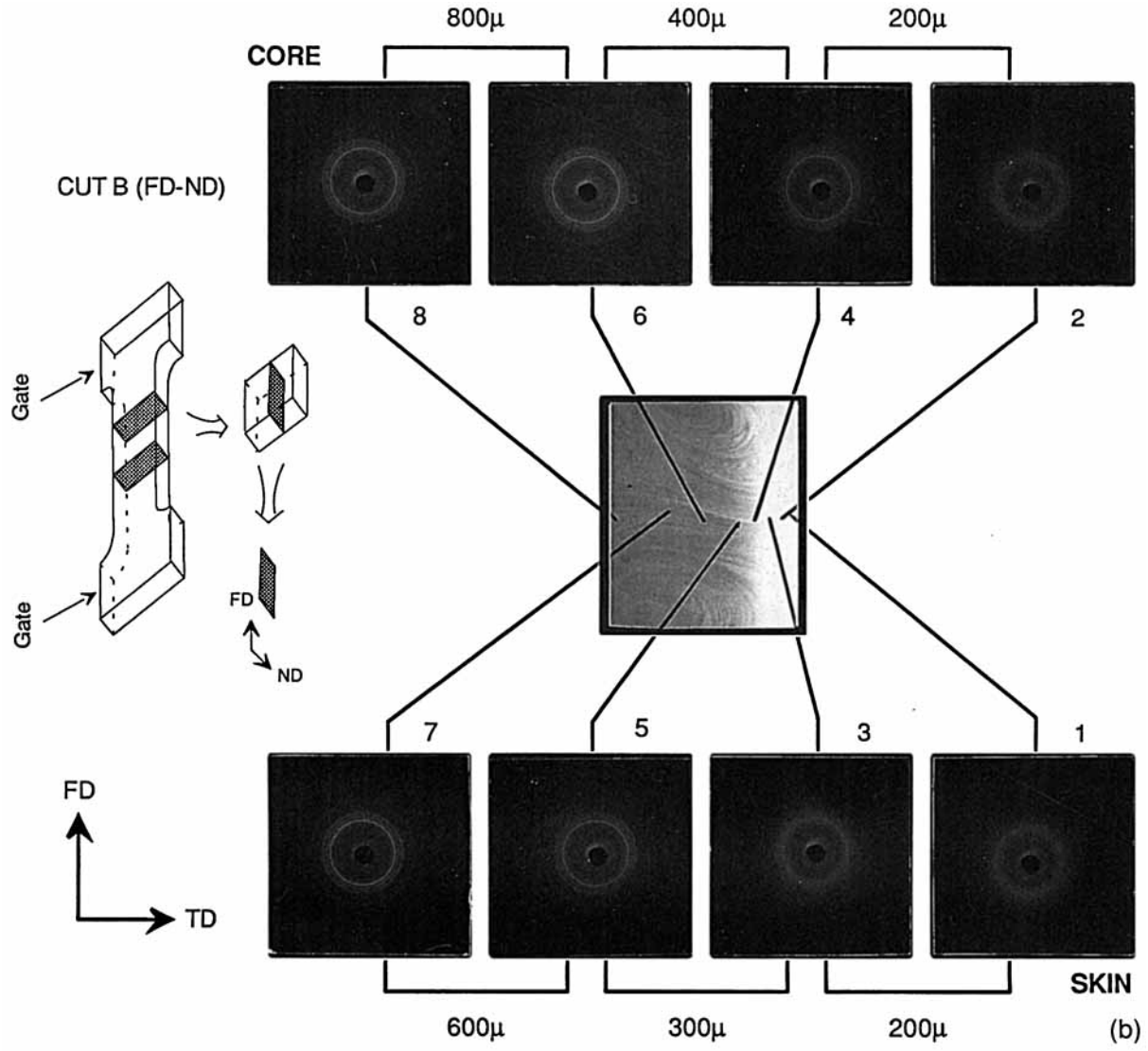

Figure 12 (*Continued from the previous page*)

regions are not only oriented as evidenced by the presence of birefringence but also possess higher crystallinity and/or crystal perfection or size.

Micro Beam X-ray Diffraction Studies

To investigate the origin of the layer formations we took a C cut of a small region near the surface upstream from the weld zone and took a series of WAXD patterns. These are displayed in Figure 11 along with the negative of the optical photomicrograph showing the exact locations where the MMBWAXD patterns were obtained. The MMBWAXD patterns taken from the layers that appear dark on the negative picture 300 and 750 mm (actually translucent) show an amorphous halo. Whereas, in the regions that appear light (actually opaque), weak but distinct crystalline diffraction rings are observed. From this view (FD–TD) the crystalline regions appear unoriented as evidenced by relatively uniform distribution of diffraction intensity in the azimuthal direction. These data clearly demonstrate that the dark–light layers observed in optical micrographs are alternating amorphous (or low crystallinity) and semicrystalline regions. We have also investigated the orientation gradients in the samples through the weld line, particularly to determine how much of the orientation developed

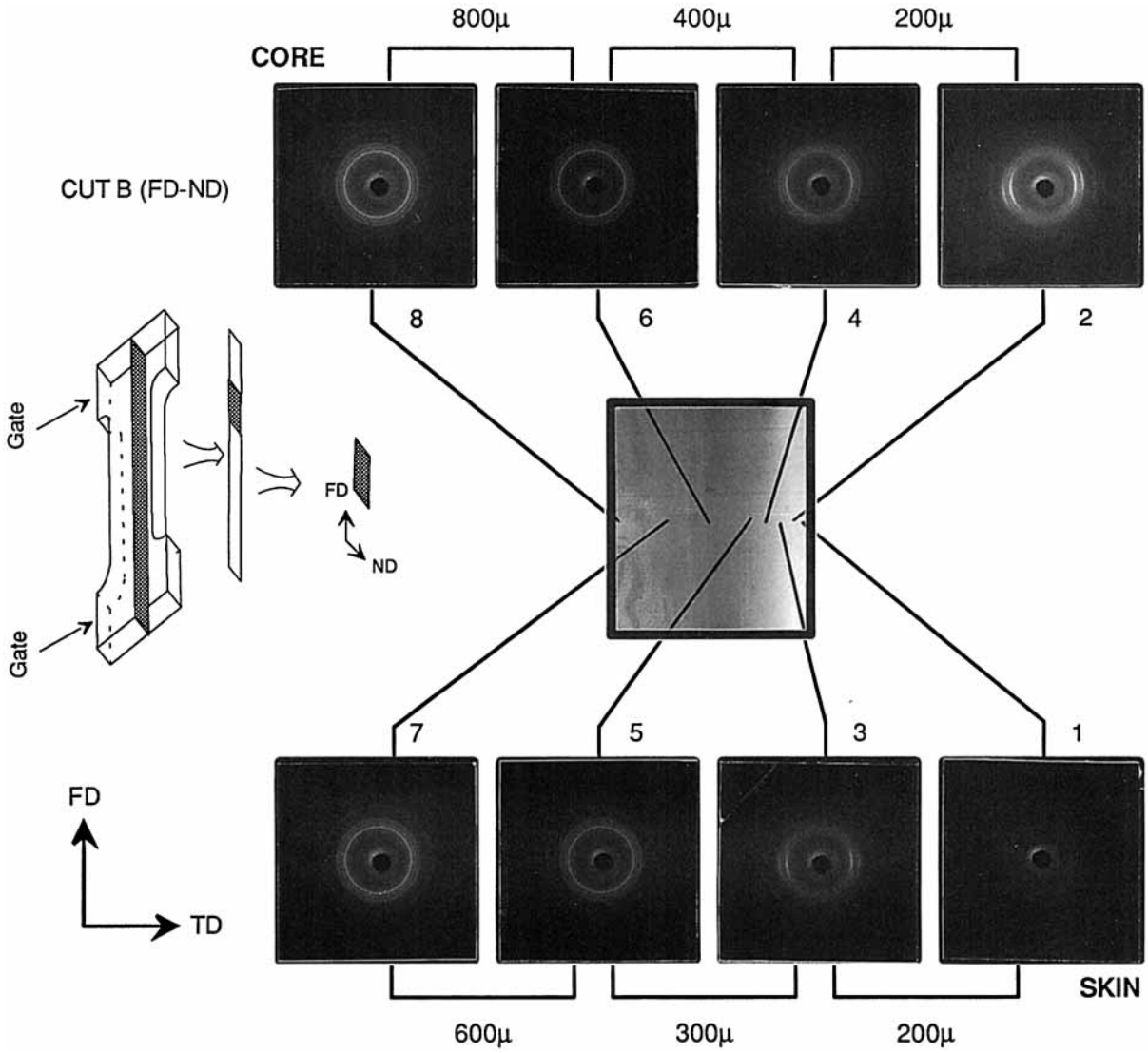

Figure 13 Micro beam wide-angle X-ray diffraction patterns through the converging region of a sample cut with procedure B. T_b = 400°C, T_m = 150°C, injection speed = 5.2 cm^3/s.

at the front surface of the fountain flow is frozen in at the weld line. For this purpose, we cut the sample using cutting procedure B and obtained the MMBWAXD patterns from skin to core along the weld line (Fig. 12). At the skin we observe an amorphous halo; however, at the interior of the sample we see crystalline rings belonging to 211, 200, 111, and 110 planes of the PAEK. The only structural differences between the samples molded with low speed [Fig. 12(a)] and those molded with high speed [Fig. 12(b)] are the thickness of the skin layer and the level of crystallinity. The sample molded with the low speed had a thicker amorphous skin layer and had less crystallinity as manifested by the low intensity of the diffraction rings. Similar results were obtained from the WAXD patterns of the weld line taken in the FD–ND and ND–TD directions. This led us to conclude that the crystalline regions at the weld line are unoriented, which is indeed expected since the weld line was formed with a relatively hot polymer supply coming from the core. MMBWAXD patterns in Figure 13 demonstrate that the converging region of the sample studied in Figure 12 indeed possesses an orientation gradient varying from skin to core.

In order to investigate the source and the cause

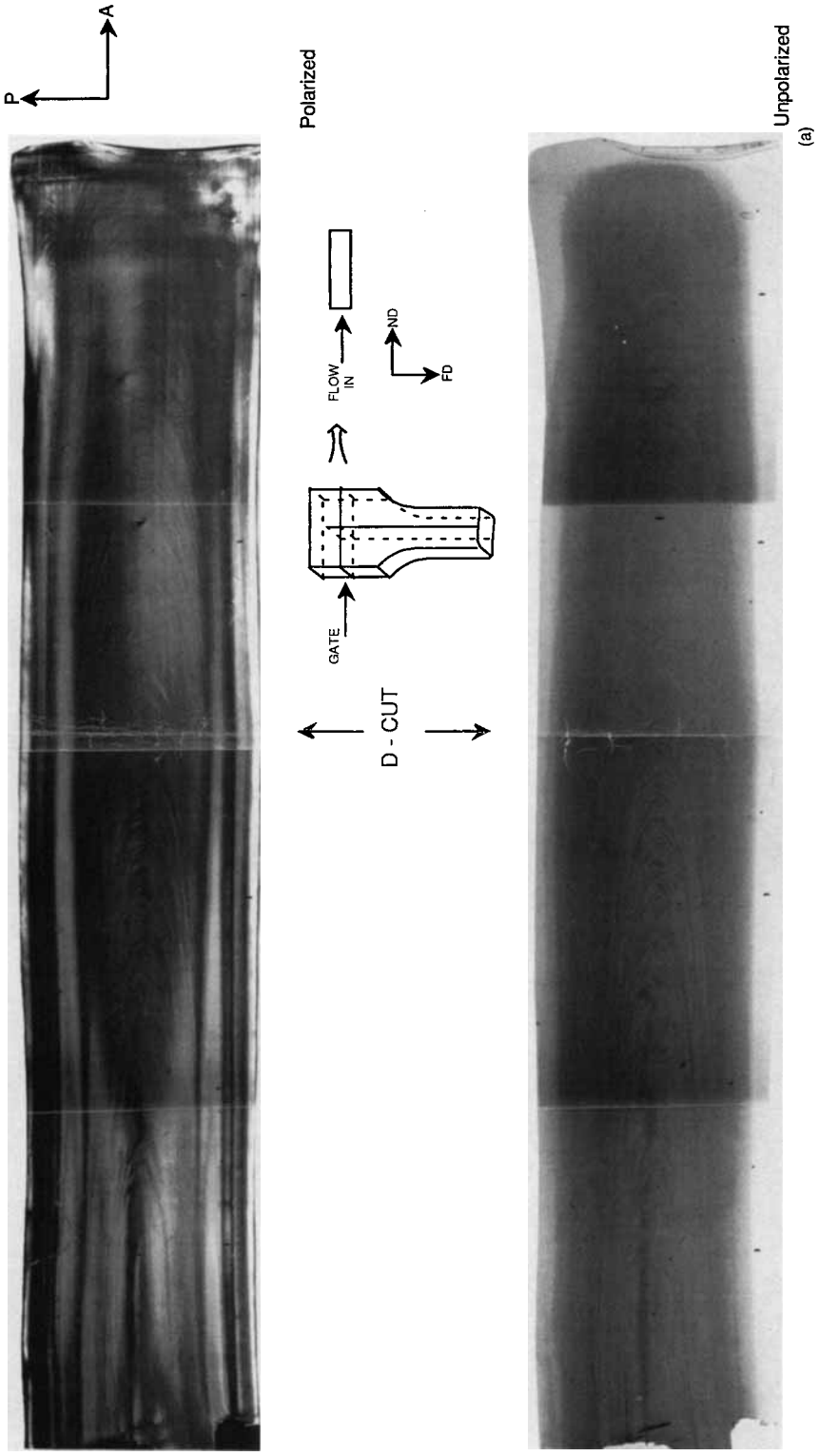

Figure 14 Polarized and unpolarized transmission light photomicrographs taken on from sample prepared at 370°C melt temperature, 20°C mold temperature and high injection speed: (a) cut D and (b) cut E.

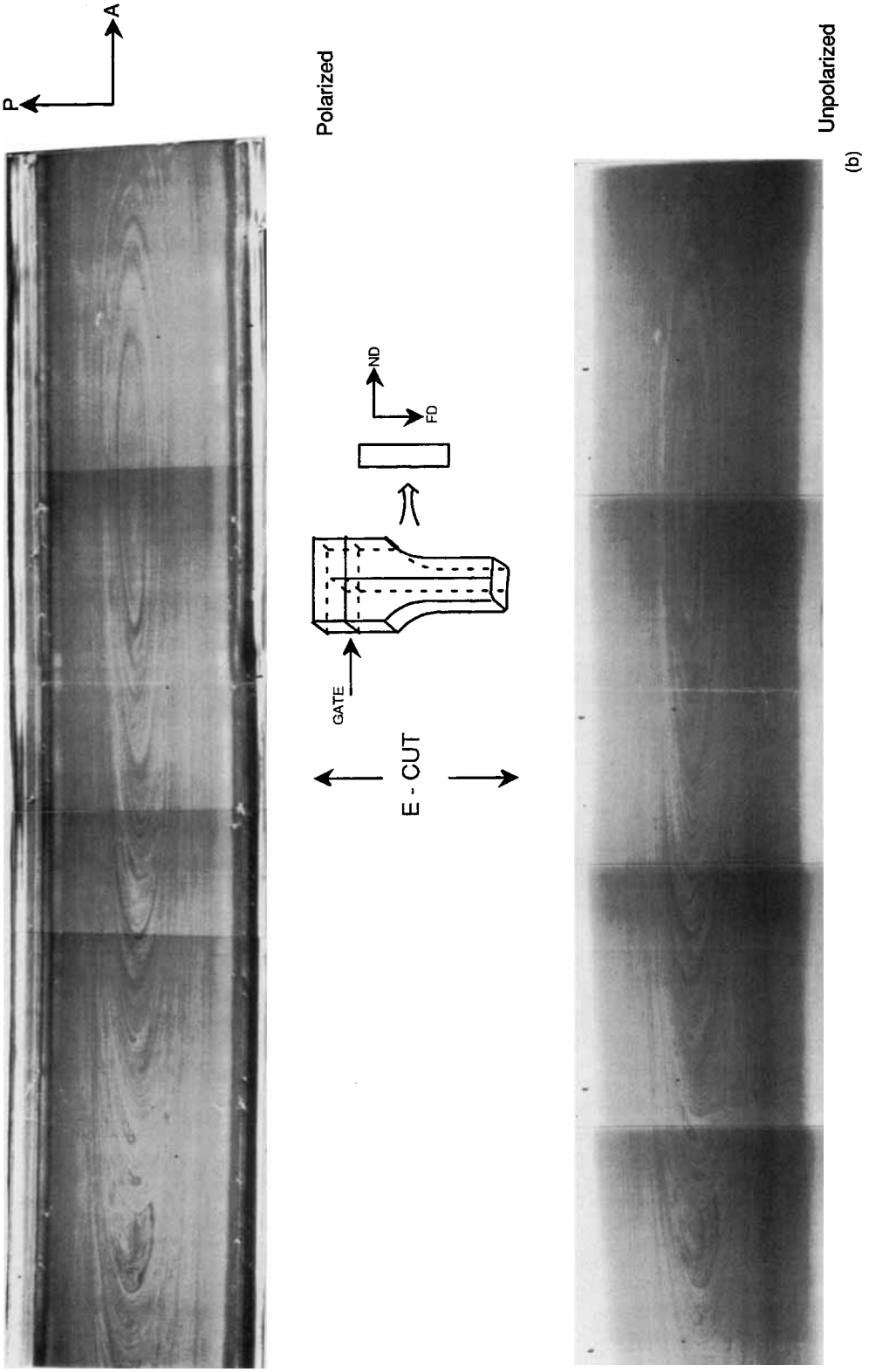

Figure 14 *(Continued from the previous page)*

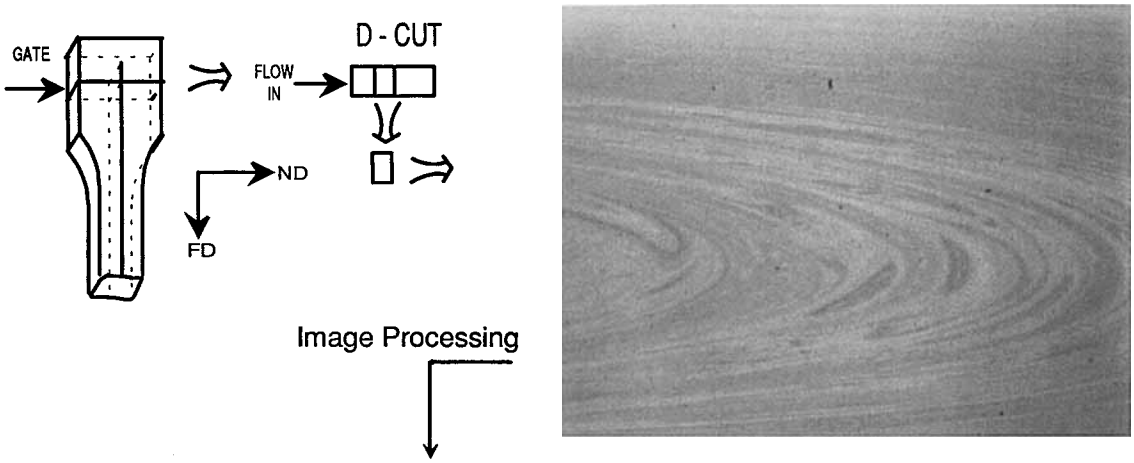

(a)

Figure 15 Binary enhancement of the dark layer lines in Figure 14.

of the alternating dark–light sequences, we selected one sample prepared at $T_b = 380°C$, $T_m = 20°C$ using the high injection speed and cut two slices, D and E, shown in Figure 14(a) and 14(b). In these figures both polarized and unpolarized photomicrographs of the same regions are shown in order to distinguish the dark–light layer sequences from the birefringence interference lines. Figure 14(a) shows the development of typical parabolic lines expected along the flow direction. Near the gate, however, these parabolic lines are irregular in shape implying that they have undergone distortions as a result of creeping flow during the packing stage. These irregular shapes occur near the core whereas the line shapes are rather uniform toward the skin. This indicates that the material near the skin had solidified before creeping flow that occurs during the packing stage distorted the lines in the core.

Another feature of the core region is that these dark regions have become segmented while maintaining their geometrical registry with the parabolic profile. Binary image enhancement of this region,

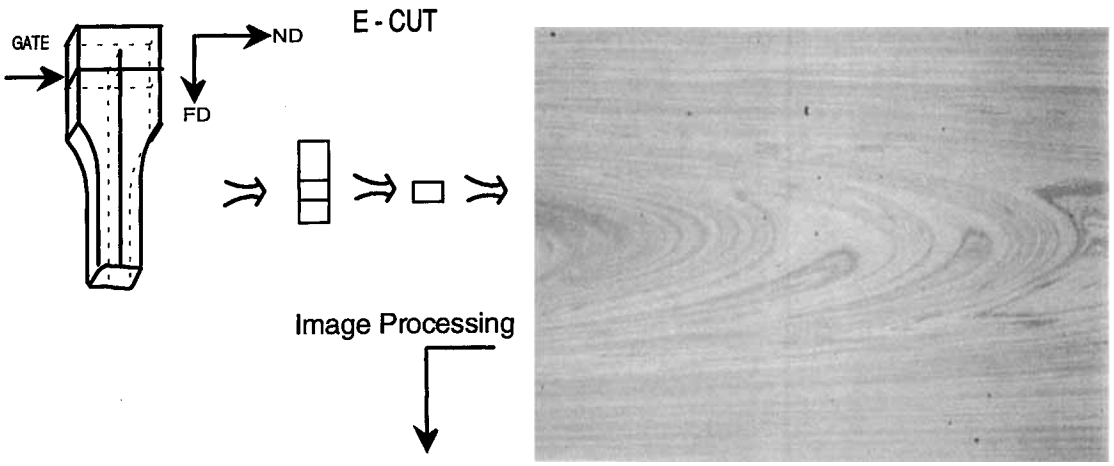

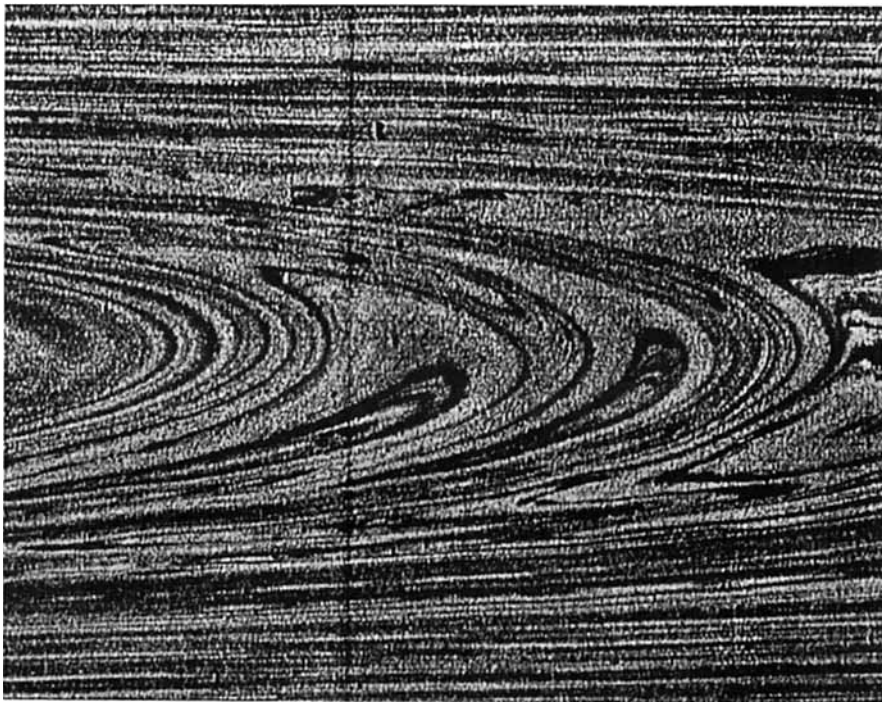

Figure 15 *(Continued from the previous page)*

which is near the gate in cut D, is shown in Figure 15(a). This suggests that the dark line sequences formed earlier in time scale (as well as up stream) and were wholly or partially carried down stream to their final position. The flow during the packing stage is only effective at the core, and its effectiveness increase toward the gate further causes the deformation of these lines.

Cut E shown in Figure 14(b) clearly shows the elliptically shaped dark–light sequences. Since this cut is normal to the local flow direction (in this region the flow direction is in the TD), the normal cut of a parabolic front would appear elliptical as shown schematically in Figure 16. Beyond this point the flow makes a 90° bend toward the major axis of the dumbbell, and in these regions we also see incomplete parabolic lines at the interior [Fig. 15(b)]. The shape of these regions suggest that they may have formed upstream and deformed during the course of flow.

We currently do not know the exact mechanism leading to the formation of these dark–light alter-

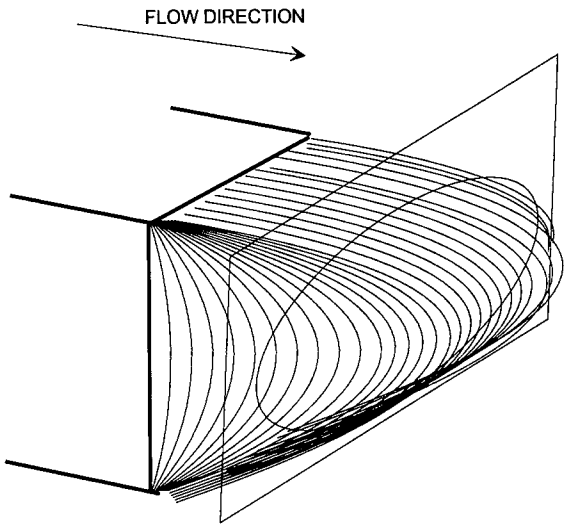

Figure 16 Formation of elliptical lines at the front of the parabolic profile.

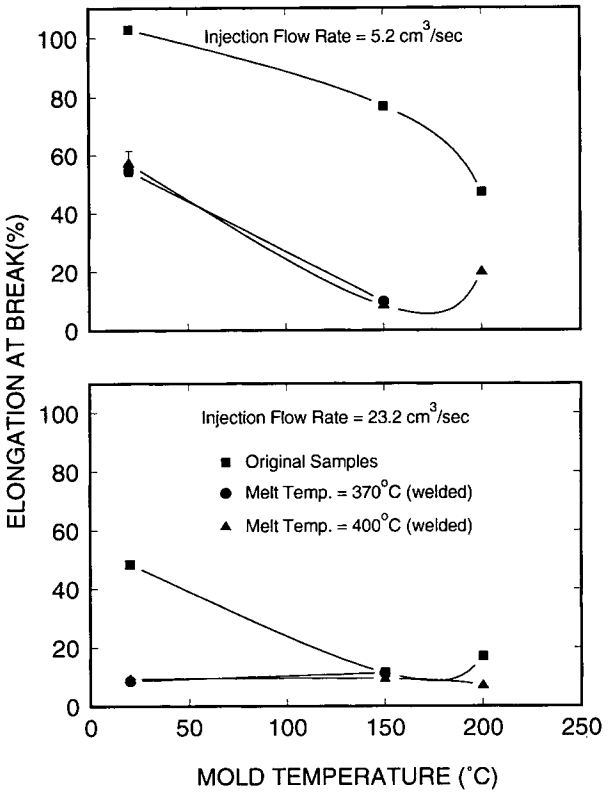

Figure 18 Elongation to break as a function of mold temperature.

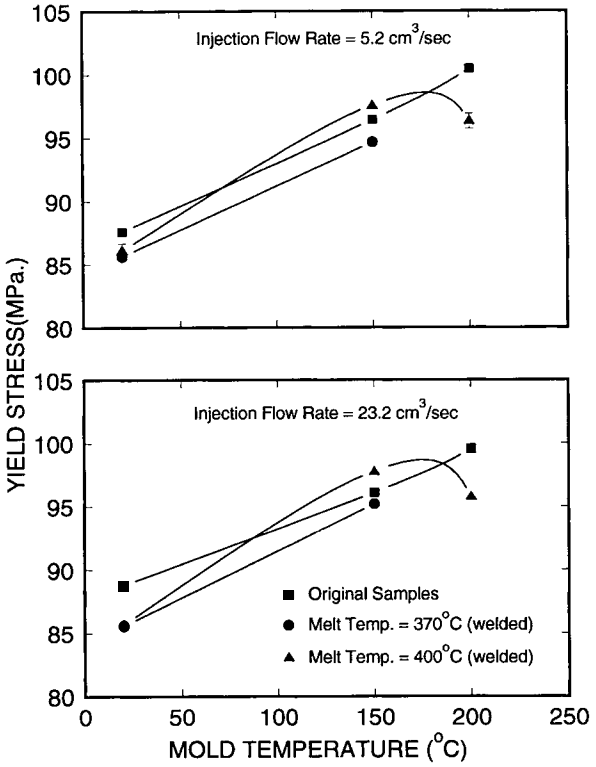

Figure 17 Yield stress as a function of mold temperature.

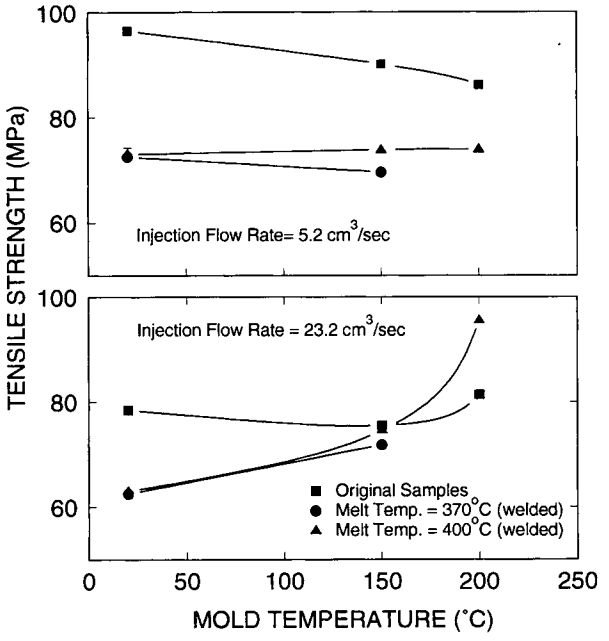

Figure 19 Tensile strength as a function of mold temperature.

nating structural sequences form. The experimental evidence suggest that they are formed upstream, most possibly in the runners and gates where they experience significant shearing and temperature gradients before they enter the cavity.

Mechanical Properties

Tensile Strength

As shown in Figure 17(a), yield stress increases with the increase of mold temperature in unwelded (designated as original samples) and samples welded at 370 and 400°C melt temperatures. In both low and high injection speeds we observe a slight decrease in yield strength between 150 and 200°C mold temperature. Injection speed seems to have a small effect on the yield stress values as demonstrated in Figure 17(b).

As a result of the increase of crystallinity, elongation to break decreases with the increase in mold temperature (Fig. 18). In this data, we clearly see the weld line effect. Welded samples exhibit significantly lower elongation at break values as compared to the original unwelded samples particularly in the samples molded with low injection speed. These values, however, are still above the values exhibited by the samples molded using higher injection speeds as indicated in the lower graph in Figure 18. We do not see a significant melt temperature effect in these figures.

Figure 19 shows the tensile strength data, welded samples exhibit lower tensile strength in low-speed molded samples, and higher melt temperature results in slightly higher tensile strength in the welded samples. At high injection speed, increasing the mold temperature and melt temperature causes a significant increase in the tensile strength particularly at 200°C mold temperature. This is mostly due to the increase of interdiffusion of chains across the weld interface at high temperatures.

Impact Strength

We determined the izod impact strength with the tip of the notch cut at the weld line (Fig. 20). These data were quite surprising at first glance; the notched impact strength of the welded specimens is consistently higher than the unwelded specimen. They decrease slightly above the 150°C mold temperature where the unwelded samples show slight maxima in the impact strength. Higher melt temperature results in slightly higher impact strength at a given processing condition, but this parameter should be considered secondary.

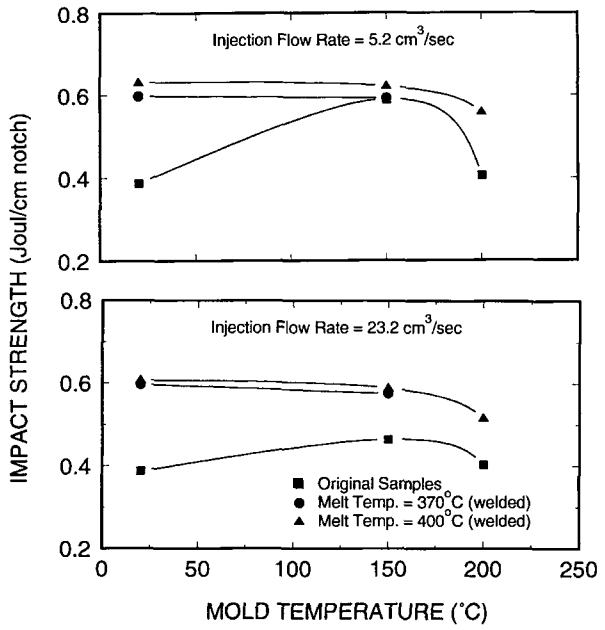

Figure 20 Notched izod impact strength as a function of mold temperature.

Fracture surfaces of unwelded and welded samples are shown in Figure 21(a) and 21(b) for two injection speeds. As one can see, the welded sample surfaces exhibit radial tear lines whose focal point are located at the initiation of the fracture (left of these pictures). The fracture surfaces of samples possessing no weld line are generally smoother than those having a weld line.

CONCLUSIONS

The weld line formed in a double gated cavity simulates the weld line formation in the race track effect. Contrary to amorphous and rapidly crystallizing polymers, in PAEK the flow patterns at the weld zone were conserved even at high mold and barrel temperatures, causing a quite complex internal structure. This was attributed to two factors in the case of PAEK:

1. When the two melt fronts meet, the supply of hot melt (having a short relaxation time) from the core due to the fountain flow pro-

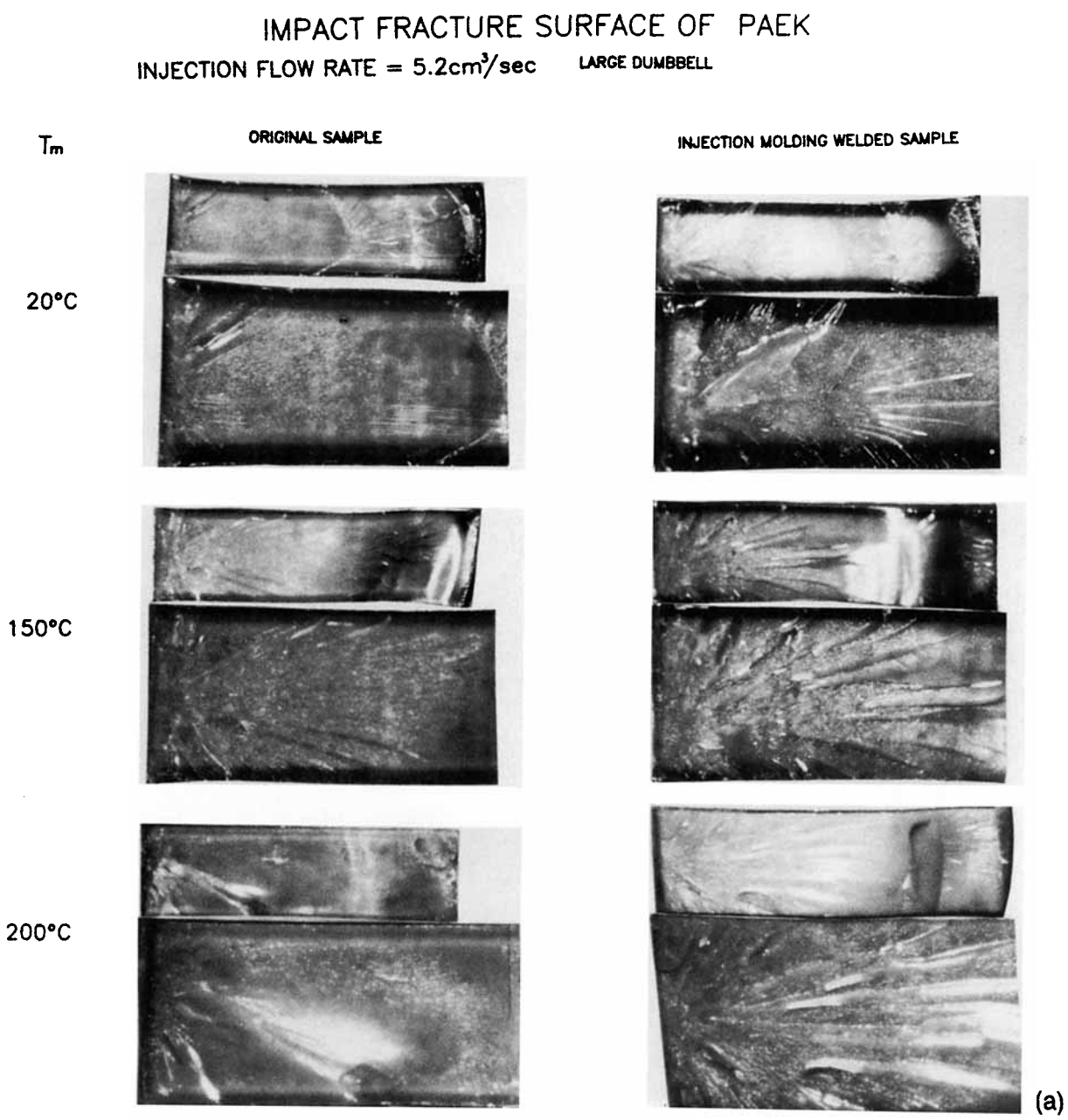

Figure 21 Fracture surfaces of impact tested samples (T_b = 400°C). (a) Samples prepared with low injection speed. (b) Samples prepared with high injection speed.

vides a good fusion and isotropy in the weld zone.

2. The processing temperature of the PAEK is relatively high (370–400°C) and its thermal conductivity and thermal crystallization rate is low. Within the short molding cycle only PAEK, which has enough accumulated thermal (weld region) and mechanical (upstream from weld region) history, crystallizes.

As we have demonstrated in this study, the PAEK exhibit multilayer formations. The number of these alternating layers increase with decreasing injection speed—making the fountain effect more pro-

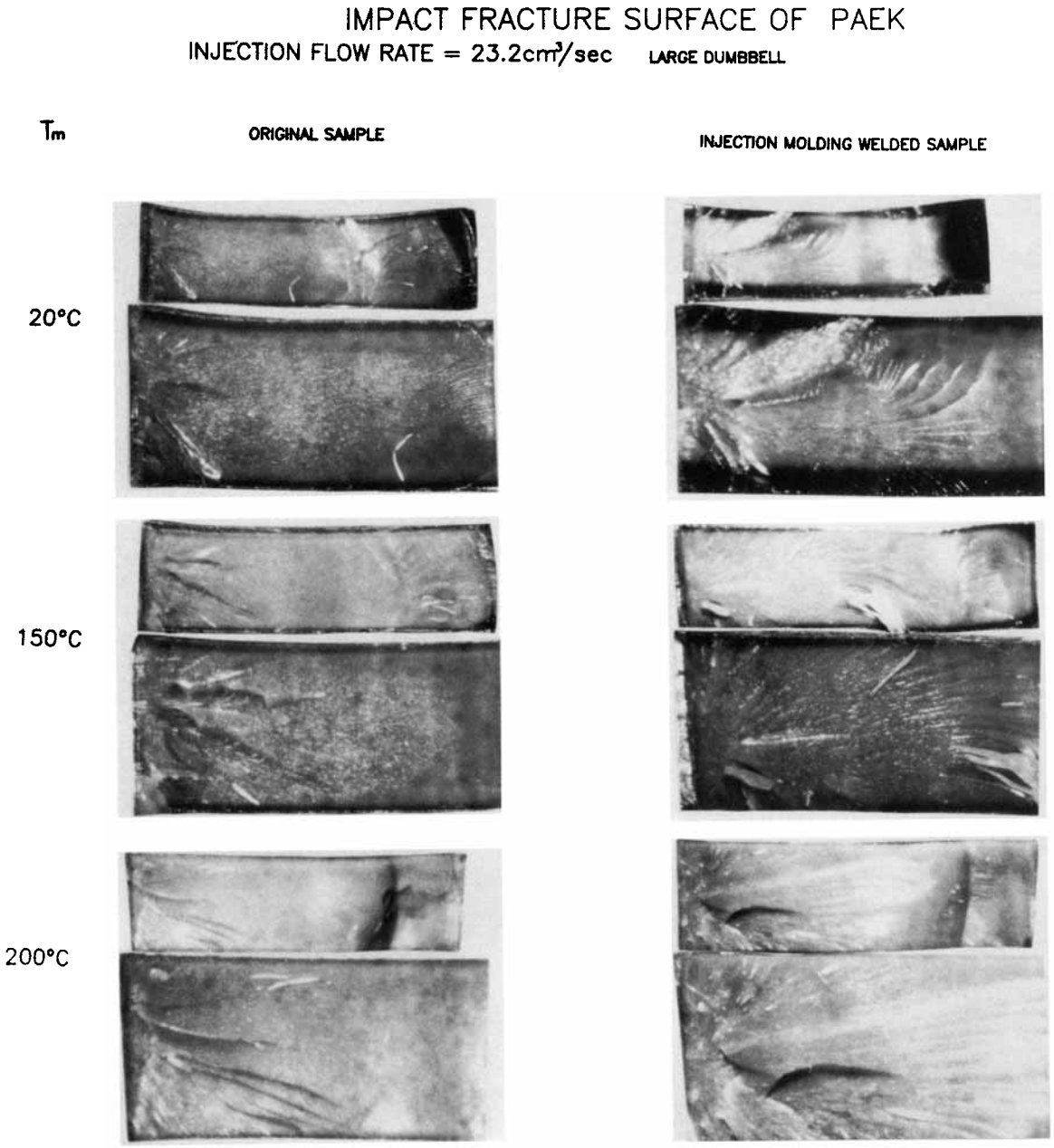

Figure 21 *(Continued from the previous page)*

nounced—or with decreasing melt temperature at low mold temperatures. These lines apparently are formed as a result of highly localized shearing history variations. The MMBWAXD patterns taken from alternating dark and light layers, as well as on-line melting studies showed that these are regions of high and low crystallinity, respectively.

We observed an unexpected increase in the impact strength in the welded samples as compared to the unwelded samples. This was attributed to the advantageous arrangement of the local structure at the weld line when two melt fronts meet.

The most affected property we found is the elongation at break, which decreases with the increase of mold temperature and when the weld line is present. Increase of melt temperature improves the ten-

sile strength particularly above 150°C mold temperature.

This research is funded by National Science Foundation Presidential Young Investigator award (Grant # DMC-8858303).

REFERENCES

1. S. Y. Hobbs, *Polym. Eng. Sci.*, **14**(9), 621 (1974).
2. S.-G. Kim and N. P. Suh, *Polym. Eng. Sci.*, **26**(17), 1200 (1986).
3. C. M. Hsiung and M. Çakmak, *J. Appl. Polym. Sci.*, **47**, 125 and 149 (1993).
4. C. M. Hsiung, M. Çakmak, and J. L. White, *Int. Polym. Proc.*, **5**(2), 109 (1990).
5. C. M. Hsiung, M. Çakmak, and J. L. White, *Polym. Eng. Sci.*, **30**(16), 967 (1990).
6. C. M. Hsiung and M. Çakmak, *Polym. Eng. Sci.*, **31**(3), 172 (1991).

Received May 23, 1994
Accepted September 6, 1994